Hexarhodium Clusters in NaY Zeolite: Characterization by Infrared and Extended X-ray Absorption Fine Structure Spectroscopies

W. A. Weber and B. C. Gates*

Department of Chemical Engineering and Materials Science, University of California, Davis, California 95616

Received: July 15, 1997; In Final Form: September 11, 1997[⊗]

Molecular clusters of rhodium were synthesized in the cages of NaY zeolite by decarbonylating supported rhodium carbonyls, which were predominantly $[Rh_6(CO)_{16}]$ prepared by carbonylation of adsorbed $[Rh(CO)_2(acac)]$ at 125 °C. The samples were characterized by infrared and X-ray absorption fine structure spectroscopies. $[Rh_6(CO)_{16}]$ formed at 125 °C, with a higher yield observed for the clusters in the uncalcined zeolite than for those in the calcined zeolite. Rhodium clusters formed by decarbonylation of $[Rh_6(CO)_{16}]$ in calcined NaY zeolite in the presence of He at temperatures of 200, 250, or 300 °C were characterized by Rh−Rh coordination numbers of approximately 3.7, indicating that the octahedral metal frame of the $[Rh_6(CO)_{16}]$ precursor remained nearly intact. When the decarbonylation of $[Rh_6(CO)_{16}]$ took place in the presence of H_2, partially decarbonylated rhodium clusters formed at 200 °C, having a Rh−Rh coordination number of about 3.6. Higher-temperature treatments in H_2 resulted in the sintering of rhodium. When $[Rh_6(CO)_{16}]$ in uncalcined NaY zeolite was decarbonylated in the presence of He, it led to the formation of particles with a Rh−Rh coordination number of 7.4, indicating that the rhodium aggregated and migrated through the zeolite pores. Thus, the water in the zeolite that favors the formation of $[Rh_6(CO)_{16}]$ in high yields causes a loss of the cluster framework during subsequent decarbonylation. The clusters that had been partially decarbonylated in H_2 at 200 °C were recarbonylated to reconstitute $[Rh_6(CO)_{16}]$, but the clusters that had been formed by decarbonylation in He at the same temperature could not be reversibly recarbonylated. The important result is that fully or partially decarbonylated rhodium clusters, consisting of about six atoms each, on average, can be formed by the decarbonylation of $[Rh_6(CO)_{16}]$ in the presence of He or H_2, respectively, and the decarbonylation chemistry is dependent on the zeolite water content.

Introduction

Metal clusters have drawn wide interest for their potential catalytic applications.[1] Practical metal cluster catalysts, exemplified by platinum in the pores of zeolite LTL,[2] are stabilized on supports; these supported platinum clusters have been found by extended X-ray absorption fine structure (EXAFS) spectroscopy to have nuclearities (numbers of metal atoms) in the range of about 5−12.[3] Attempts to understand how cluster size affects catalytic properties have motivated the preparation of supported clusters with nearly uniform structures, and the most effective synthetic method involves preparation of supported metal carbonyl clusters as precursors followed by removal of the CO ligands without substantial changes in the metal frame.[4] Zeolites appear to be the preferred supports because their small uniform cages may favor the formation of small uniform clusters.[5]

For example, $[Rh_6(CO)_{16}]$ was synthesized in the pores of NaY zeolite by reductive carbonylation of species formed from rhodium salts,[6−10] and $[Ir_4(CO)_{12}]$ and $[Ir_6(CO)_{16}]$ were formed in this zeolite from $[Ir(CO)_2(acac)]$ (acac is acetylacetonate).[11] Upon decarbonylation, the iridium clusters formed from $[Ir_6(CO)_{16}]$ were found by EXAFS spectroscopy to be nearly Ir_6.[12] However, there is hardly any literature of clusters formed by decarbonylation of cluster carbonyls other than iridium.

Our goal was to prepare uniform supported rhodium clusters; the precursor was chosen to be $[Rh_6(CO)_{16}]$ in NaY zeolite. We report the synthesis and characterization of $[Rh_6(CO)_{16}]$ by a new method and the characterization of a family of decarbonylated and recarbonylated rhodium clusters based on infrared and EXAFS spectroscopies.

Experimental Section

Materials and Sample Preparation. Syntheses and sample transfers were conducted with exclusion of air and moisture on a double-manifold Schlenk vacuum line and in a N_2-filled Vacuum Atmospheres drybox. N_2, H_2, and He with purities of 99.999% passed through traps containing particles of Cu and molecular sieve zeolite to remove traces of O_2 and moisture. CO (Puritan Bennett, UHP grade) passed through a similar trap. Hexanes and pentanes (Fisher, HPLC grade) were dried over sodium benzophenone ketyl and then deoxygenated by purging with flowing N_2 for 2 h. Tetrahydrofuran (THF) (Fisher, HPLC grade) was dried over sodium benzophenone ketyl and deoxygenated prior to use. $CHCl_3$ (Fisher, HPLC grade), $[Rh(CO)_2(acac)]$ [dicarbonylacetylacetonato rhodium (I)] (Strem, 99%), $[Rh_6(CO)_{16}]$ (Strem, 98%), and $[Rh_2O_3]$ (anhydrous, Strem, 99.9%) were used as received.

NaY zeolite (W. R. Grace and Co.) was either evacuated for 12 h or calcined (at temperatures of 200 or 300 °C) and then brought in contact with a solution of $[Rh(CO)_2(acac)]$ to yield a sample containing 2.25% Rh. In each preparation, the support was slurried with the precursor in dried hexanes or pentanes in a Schlenk flask under N_2. After the slurry was stirred at room temperature for several days, the solvent was removed by evacuation and the solid dried in vacuo (pressure $<10^{-3}$ Torr) overnight. The resulting solids were stored in the drybox.

Samples were carbonylated in a flow reactor with CO at 2 atm (or 1 atm when the reactor was an infrared cell) and were decarbonylated in an EXAFS cell at 1 atm in flowing H_2 or He.

Infrared Spectroscopy. Transmission infrared spectra of the samples were collected with a Bruker IFS-66V spectrometer with a spectral resolution of 0.1 cm^{-1}. Samples of the supported

* Address correspondence to this author.
[⊗] Abstract published in *Advance ACS Abstracts,* November 1, 1997.

S1089-5647(97)02310-9 CCC: $14.00

TABLE 1: Crystallographic Data Characterizing the Reference Compounds and Fourier Transform Ranges Used in the EXAFS Data Analysis[a]

		crystallographic data			Fourier transform[a]		
ref cmpd	shell	*N*	*r*, Å	ref	Δk, Å^{-1}	Δr, Å	*n*
Rh foil	Rh−Rh	12	2.687	17	2.86−19.60	1.62−3.12	3
Rh_2O_3	Rh−O	6	2.050	18	2.67−15.69	0.00−2.10	2
$[Ru_3(CO)_{12}]$	Rh−C	4	1.910	19	3.71−14.80	0.95−1.87	1
	Rh−O*	4	3.050	19	3.75−14.80	1.90−3.11	2

[a] Notation: *N*, coordination number characterizing absorber−backscatterer pair; *r*, distance; Δk, limits used for forward Fourier transformation (*k* is the wave vector); Δr, limits used for shell isolation; *n*, power of *k* used for Fourier transformation.

precursors and samples prepared by carbonylation were pressed into thin self-supporting wafers in the drybox and loaded into a controlled-atmosphere infrared cell. Purified He, H_2, or CO flowed through the cell. Each sample was scanned 64 times and the signal averaged.

Attempted Extraction of Metal Carbonyls from NaY Zeolite. Attempts were made to extract rhodium carbonyls from NaY zeolite samples by contacting the samples with freshly distilled THF under N_2. The supernatant liquid was transferred by syringe into a solution infrared cell and quickly scanned.

EXAFS Data Collection. The EXAFS experiments were performed on X-ray beam line X-11A at the National Synchrotron Light Source at Brookhaven National Laboratory, Upton, NY. The storage ring operated at an energy of 2.5 GeV with ring currents between 140 and 240 mA.

Transmission EXAFS experiments were carried out with wafers prepared in a N_2-filled glovebox at the synchrotron. A powder sample was placed in a holder in the glovebox, which was then placed in a die and pressed into a self-supporting wafer. The wafer was loaded into an EXAFS cell[13] and sealed. Typically, the cell was evacuated immediately after removal from the glovebox.

EXAFS spectra were recorded with the sample under vacuum and cooled with liquid N_2; the sample temperature was approximately 120 K. Higher harmonics in the X-ray beam were minimized by detuning the Si(111) double-crystal monochromator by 15−20% at the Rh K edge (23 220 eV). Details of the experiments are as reported elsewhere.[14]

EXAFS Data Analysis

EXAFS Reference Data. The EXAFS data were analyzed with experimentally determined reference files obtained from EXAFS data for materials of known structure. The Rh−Rh and Rh−$O_{support}$ interactions were analyzed with phase shifts and backscattering amplitudes obtained from EXAFS data for Rh foil and Rh_2O_3, respectively. The Rh−C and Rh−O* (O* refers to carbonyl oxygen) interactions were analyzed with phase shifts and backscattering amplitudes obtained from EXAFS data characterizing crystalline $[Ru_3(CO)_{12}]$ (which has only terminal CO ligands) mixed with BN. The transferability of the phase shift and backscattering amplitudes for neighboring atoms in the periodic table has been justified experimentally.[15] $[Ru_3(CO)_{12}]$ was chosen because the multiple scattering effect in the Rh−O* shell is significant as a consequence of the near linearity of the Rh−C−O moieties, and it was necessary to fit the data with a reference that exhibits multiple scattering.[16] The parameters used to extract these files from the EXAFS data are summarized in Table 1. Details of the preparation of the reference files are presented elsewhere.[20−22]

TABLE 2: Summary of EXAFS Analyses

sample	no. of scans	std dev in EXAFS function[a]	*k* range, Å^{-1}	*r* range, Å	*p*[b]
$[Rh_6(CO)_{16}]$ mixed with BN	2	0.004	4.2−14.7	0−5	34
$[Rh_6(CO)_{16}]$ in NaY zeolite[c]	5	0.004	4.2−14.7	0−5	34
Rh clusters in NaY zeolite formed by decarbonylation of $[Rh_6(CO)_{16}]$ in He[d,e]	2−6	0.001	4.1−14.7	0−5	34
Rh clusters in NaY zeolite formed by decarbonylation of $[Rh_6(CO)_{16}]$ in H_2[e,f]	2−6	0.001	4.1−14.7	0−5	34

[a] Standard deviation estimated from data characterizing a similar sample that had been scanned six times. [b] Statistically justified number of free parameters calculated from the Nyquist theorem, $p = 2\Delta k\Delta r/\pi + 1$. [c] $[Rh_6(CO)_{16}]$ in mixture with other rhodium carbonyls; see text for details. [d] See text for details. [e] Several separate samples characterized, with number of scans per sample varying from one sample to another. [f] Cluster only partially decarbonylated; see text for details.

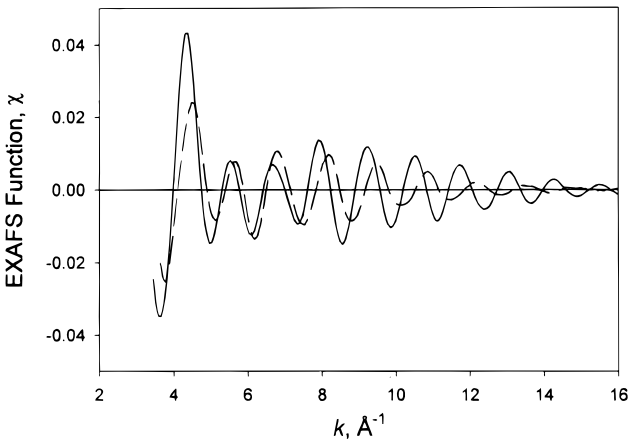

Figure 1. Raw EXAFS data characterizing NaY zeolite-supported rhodium carbonyl clusters formed from $[Rh(CO)_2(acac)]$ in flowing CO at 125 °C and 2 atm for 12 h (solid line) and sample decarbonylated at 200 °C in flowing H_2 (dashed line).

Decarbonylated Samples Formed from Rhodium Carbonyl-Containing NaY Zeolite. EXAFS data from two to six scans were averaged for each sample (Table 2). The normalized EXAFS functions were obtained from the averaged X-ray absorption spectra by a cubic spline background subtraction and normalized by division by the edge height (e.g., Figure 1). In the intermediate and higher ranges of the wave vector *k* ($8 < k < 16$ Å), there are strong oscillations characteristic of metal−metal interactions in each sample, consistent with the presence of metal clusters or particles.

In the EXAFS analysis, no attempt was made to smooth the data. With the difference file technique,[22,23] the Rh−Rh contribution, the largest in the EXAFS spectrum, was estimated by calculating an EXAFS function that agreed as closely as possible in *r* space ($1.5 < r < 3.5$ Å; *r* is the absorber−backscatterer distance) with the k^0-weighted data characterizing the high-*k* range ($8 < k < 14.6$ Å^{-1}); the metal−support contributions in this high-*k* range are small because the backscatterers in the support have low atomic weights relative to that of Rh. An EXAFS function calculated with the first-guess parameters was subtracted from the full data. The residual spectrum was expected to account for Rh−$O_{support}$, Rh−C, and Rh−O* interactions, representing any residual carbonyl ligands or carbonaceous species resulting from the acac ligands in the precursor $[Rh(CO)_2(acac)]$. The difference file was estimated with two Rh−O contributions (one of them characterized by multiple scattering) and with one Rh−C contribution. All the

TABLE 3: ν_{CO} Stretching Frequencies of Rhodium Carbonyls in Solution and Supported on NaY Zeolite

sample	terminal CO stretching frequency, cm^{-1}	bridging CO stetching frequency, cm^{-1}	ref
$[Rh(CO)_2(acac)]$ in calcined NaY zeolite	2014 s, 2082 s		this work
$[Rh(CO)_2(acac)]$ in uncalcined NaY zeolite	2023 s, 2092 s		this work
$[Rh_6(CO)_{16}]$ in NaY zeolite[a]	2095 s, 2066 sh, 2045 sh, 2020 w	1764 s	6
$[Rh_6(CO)_{16}]$ in NaY zeolite[a]	2098 s, 2066 w	1760 s	7
$[Rh_6(CO)_{16}]$ in NaY zeolite[a]	2099 s, 2069 w, 2020 w	1765 s	9, 10
$[Rh_4(CO)_{12}]$ in NaY zeolite[a]	2086 vs, 2069 sh, 2050 sh, 2025 sh	1834 s	9, 10
$[Rh_6(CO)_{16}]$ in untreated NaY zeolite[b]	2130 w, 2092 s, 2067 sh, 2020 w	1768 s	this work
$[Rh_6(CO)_{16}]$ in NaY zeolite calcined at 200 °C[b]	2130 w, 2097 s, 2068 sh, 2020 w	1760 s	this work
$[Rh_6(CO)_{16}]$ in NaY zeolite calcined at 300 °C[b]	2130 w, 2097 s, 2068 sh, 2020 w	1760 s	this work
Rh clusters in untreated NaY zeolite formed by decarbonylation of $[Rh_6(CO)_{16}]$ in H_2 at 200 °C	2000 sh, 1928 br		this work
Rh clusters in untreated NaY zeolite formed by decarbonylation of $[Rh_6(CO)_{16}]$ in He at 200 °C	2110 sh, 2094 w, 2047 w, 2020 w		this work
Rh clusters in untreated NaY zeolite formed by decarbonylation of $[Rh_6(CO)_{16}]$ in He at 200 °C, followed by CO at 125 °C for 12 h	2131 w, 2102 s, 2068 s, 2047 s, 2020 s	1833 w, 1768 s	this work

[a] Purity of sample unknown. [b] See text for estimate of purity.

parameters were varied until a good agreement was found between the raw and fitted data with k^0 weighting in r space.

The first-guess Rh−Rh and Rh-low Z backscatterer contributions were then added and compared with the raw data in r space; the fit was not satisfactory. Then the Rh-low Z backscatterer contributions were subtracted from the data, and a better fit for the Rh−Rh contribution was determined. The improved fit characterizing the Rh−Rh contribution was subtracted from the full EXAFS data, and better parameter estimates were determined by fitting the Rh-low Z backscatterer contributions to the residual spectrum. This process was carried out in r space with the raw EXAFS data with k^0 weighting and repeated until a good overall agreement between the Fourier transform of the raw EXAFS data and the fit in r space was obtained, with the final Rh−Rh contribution showing excellent agreement with the data not only for the k^0 weighting but also for k,[1] k,[2] and k^3 weightings.

EXAFS data characterizing clusters formed by decarbonylation in He were fitted with Rh−Rh and Rh−$O_{support}$ contributions only, whereas EXAFS data characterizing clusters formed in H_2 were fitted with Rh−Rh, Rh−$O_{support}$, Rh−C, and Rh−O* contributions. The number of parameters used to fit the data in these main-shell analyses was thus 8 or 16, respectively; the statistically justified number, estimated on the basis of the Nyquist theorem,[24] is approximately 34 for each sample (Table 2).

Rhodium Carbonyls in NaY Zeolite. The analysis of the EXAFS data characterizing the rhodium carbonyl clusters in NaY zeolite prior to decarbonylation was more complicated than that described above because there are two Rh−C and two Rh−O* contributions associated with the carbonyl ligands of clusters such as $[Rh_6(CO)_{16}]$. In crystalline $[Rh_6(CO)_{16}]$, terminal carbonyl ligands are characterized by a Rh−C−O bond angle of 176°, and face-bridging carbonyl ligands are characterized by a bond angle of 132°.[25] The analysis of these contributions is complicated by multiple scattering effects which cause the EXAFS phase shift and amplitude functions to depend strongly on the positions of the atoms.[26] Therefore, three separate fits were obtained for each of the samples containing the rhodium carbonyls, namely, $[Rh_6(CO)_{16}]$ mixed with BN, and the samples formed by carbonylation of $[Rh(CO)_2(acac)]$ in each of the following: uncalcined NaY zeolite, NaY zeolite calcined at 200 °C, and NaY zeolite calcined at 300 °C.[27] In the first fit, only one Rh−O contribution was included (with a distance of about 3 Å), with multiple scattering. In the second fit, two Rh−O contributions with multiple scattering were included, with the distances being about 2.5 and 3 Å. In the third fit, two Rh−O contributions were included, one with multiple scattering and one without. The first two fits are reported in a thesis,[27] and the third (and best) fit is reported here.

Results

Infrared Evidence of Formation of $[Rh_6(CO)_{16}]$ in NaY Zeolite. The precursor **[**$Rh(CO)_2(acac)$] in *n*-hexane solution was brought in contact with the uncalcined or calcined NaY zeolite support. The slurry was mixed for several days until no change in color of the solution was observed. When the slurry contained uncalcined NaY zeolite, the color of the solution was a faint yellow, indicating that nearly all the $[Rh(CO)_2(acac)]$ had been adsorbed. However, when calcined NaY zeolite was used, the solution became clear, indicating virtually complete uptake of $[Rh(CO)_2(acac)]$. After removal of the solvent, each solid was light gray and characterized by an infrared spectrum with two strong ν_{CO} bands; these appeared at 2092 and 2023 cm^{-1} or at 2082 and 2014 cm^{-1}, characterizing uncalcined or calcined NaY zeolite, respectively. These spectra are consistent with rhodium dicarbonyl species (Table 3).[28−31] The small peak at 1710 cm^{-1} in these spectra is attributed to acetylacetonate or species formed from these ligands.[32]

Treatment of the sample formed from $[Rh(CO)_2(acac)]$ and uncalcined NaY zeolite in flowing CO at 125 °C for 12 h led to a light pink-gray solid with an infrared spectrum (ν_{CO}: 2130 sh, 2092 s, 2067 sh, 2020 w, 1765 s cm^{-1}) similar to the spectrum of $[Rh_6(CO)_{16}]$ in chloroform solution (ν_{CO}: 2077 vs, 2046 w, 1805 m cm^{-1}) (Figure 2). The spectrum closely matches those of samples of $[Rh_6(CO)_{16}]$ in NaY zeolite synthesized by others.[7−10] Similar spectra were obtained for samples prepared from $[Rh(CO)_2(acac)]$ and calcined zeolites which had been treated in flowing CO (Figure 3). We infer that $[Rh_6(CO)_{16}]$ formed in the zeolites by carbonylation of the rhodium-containing precursor. Our method of synthesis differs from those reported as we used a different precursor, but the results are virtually the same.

Extraction of the rhodium carbonyl species from the zeolites was attempted with THF and $CHCl_3$. Because the infrared spectra of the extract solutions gave no evidence of metal carbonyls, we infer that the rhodium carbonyls were trapped in the zeolite cages.

Infrared Evidence of Decarbonylation of Rhodium Carbonyl Clusters in NaY Zeolite. Uncalcined NaY zeolite containing rhodium carbonyl clusters was treated in He at 1 atm as the temperature was ramped from room temperature to

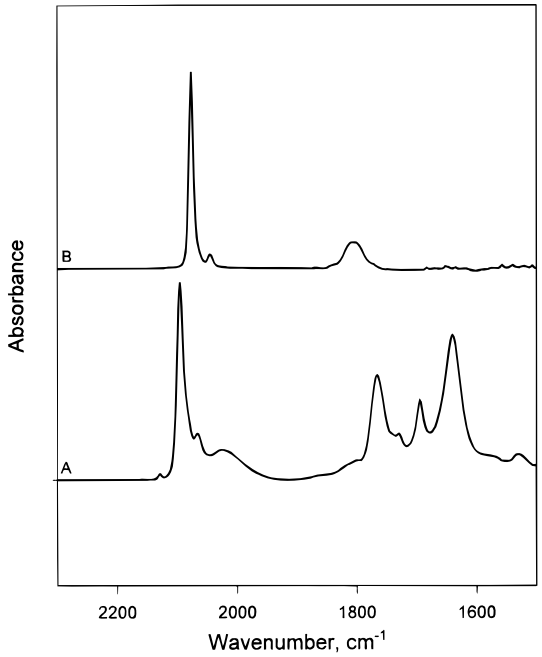

Figure 2. Infrared spectra of (A) sample prepared by treating NaY zeolite containing $[Rh(CO)_2(acac)]$ in CO at 2 atm and 125 °C for 12 h and (B) $[Rh_6(CO)_{16}]$ in chloroform solution.

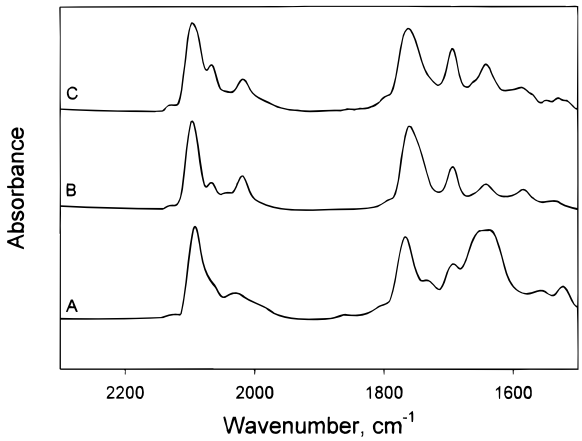

Figure 3. Infrared spectra of (A) uncalcined NaY zeolite containing $[Rh(CO)_2(acac)]$ after treatment in CO at 2 atm and 125 °C for 12 h; (B) NaY zeolite (calcined at 200 °C) containing $[Rh(CO)_2(acac)]$ after treatment in CO at 2 atm and 125 °C for 12 h; and (C) NaY zeolite (calcined at 300 °C) containing $[Rh(CO)_2(acac)]$ after treatment in CO at 2 atm and 125 °C for 12 h.

200 °C at a rate of 3 °C/min and then held for 2 h. This treatment was followed by treatments in He at 250 and 300 °C. Similarly, the samples of rhodium carbonyl-containing NaY zeolite that had been calcined at 200 or 300 °C prior to the introduction of $[Rh(CO)_2(acac)]$ were decarbonylated in He at 1 atm at 200, 250, 300, and 400 °C. The treatment of each sample in He at 200 °C led to nearly complete decarbonylation, and the decarbonylation was complete at 250 °C (Figure 4).

Uncalcined NaY zeolite containing rhodium carbonyl clusters was treated in H_2 at 1 atm as the temperature was ramped from room temperature to 200 °C at a rate of 3 °C/min and then held for 2 h. This treatment was followed by treatments in H_2 at 250 and 300 °C. The samples made from NaY zeolite that had been calcined at 200 or 300 °C were also decarbonylated in H_2 at the same temperatures. In each case, the treatment in H_2 led to the disappearance of the terminal υ_{CO} bands at 2131 sh, 2096 vs, 2067 m, and 2020 m cm^{-1}, but a new broad absorption peak

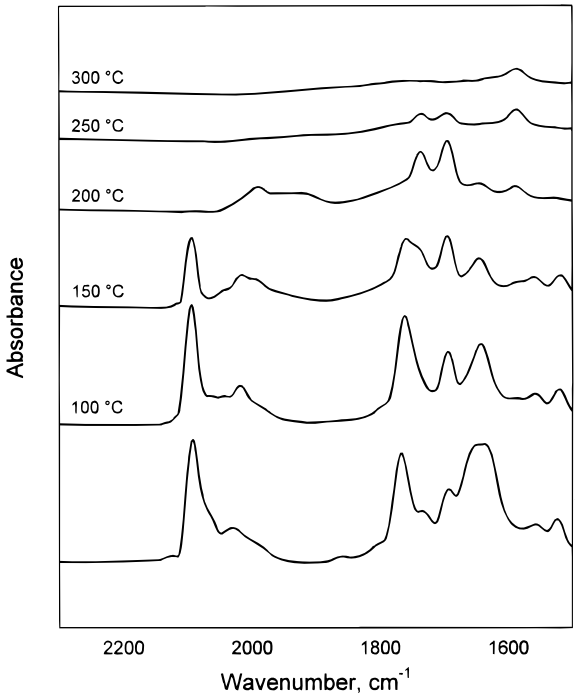

Figure 4. Infrared spectra of $[Rh_6(CO)_{16}]$ in uncalcined NaY zeolite and after treatments in He at the temperatures shown.

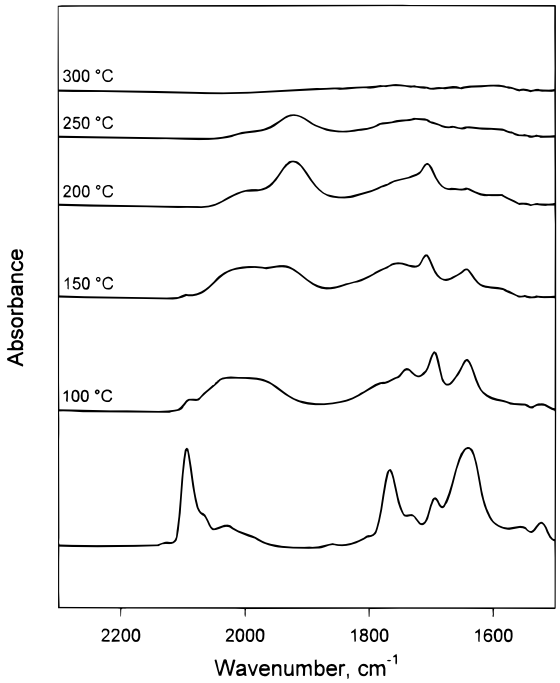

Figure 5. Infrared spectra of $[Rh_6(CO)_{16}]$ in uncalcined NaY zeolite and after treatments in H_2 at the temperatures shown.

appeared at lower frequency, centered at approximately 1930 cm^{-1}, with a shoulder at 2000 cm^{-1} (Figure 5). In each case, the peak at 1765 cm^{-1}, indicating the presence of face-bridging CO ligands, disappeared. Decarbonylation in the presence of H_2 was nearly complete at 300 °C. All partially decarbonylated and fully decarbonylated samples were gray in color.

Infrared Evidence of Recarbonylation of Decarbonylated Rhodium Clusters. With CO at 1 atm flowing through the infrared cell containing the decarbonylated clusters in uncalcined NaY zeolite, the temperature was ramped from room temperature to 125 °C and held for 12 h. The spectrum showed that the sample that had been decarbonylated in the presence of He at 200 °C was not reconverted into $[Rh_6(CO)_{16}]$. Instead, the

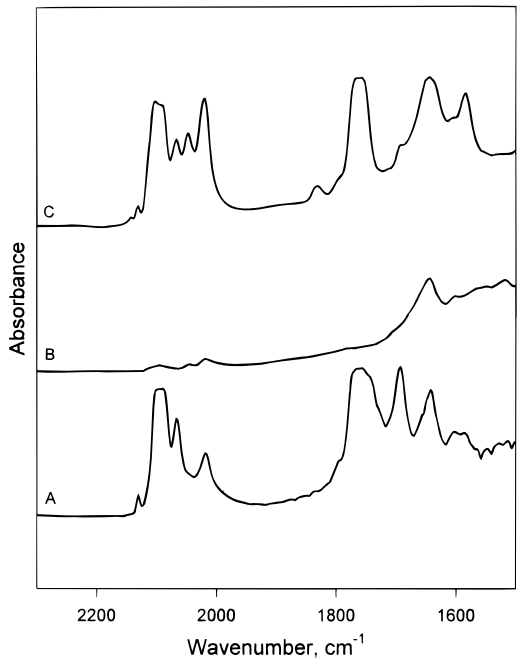

Figure 6. Infrared spectra of (A) NaY zeolite containing [$Rh(CO)_2$(acac)] treated in CO at 1 atm and 125 °C for 12 h; (B) sample of spectrum A after treatment in He at 200 °C for 2 h; and (C) sample of spectrum B followed by treatment in CO at 125 °C for 12 h.

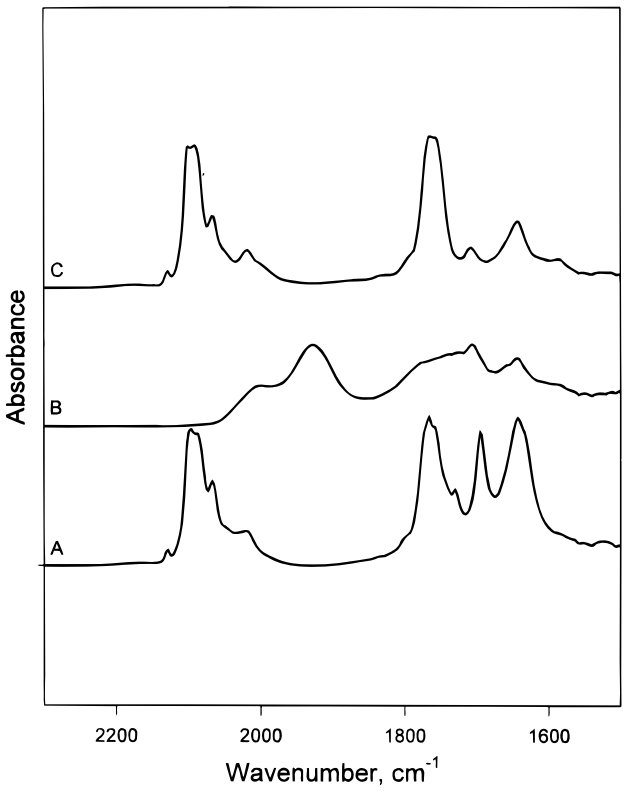

Figure 7. Infrared spectra of (A) NaY zeolite containing [$Rh(CO)_2$(acac)] treated in CO at 1 atm and 125 °C for 12 h; (B) sample of spectrum A after treatment in H_2 at 200 °C for 2 h; and (C) sample of spectrum B followed by treatment in CO at 125 °C for 12 h.

spectrum included strong terminal CO absorptions at 2131 w, 2102 s, 2068 s, 2047 s, and 2020 s cm^{-1} and bridging CO absorptions at 1833 and 1765 cm^{-1} (Figure 6). The sample was gray in color. In contrast, the sample that had been partially decarbonylated in the presence of H_2 at 200 °C was characterized by CO bands at 2130 w, 2098 s, 2068 sh, 2047 sh, and

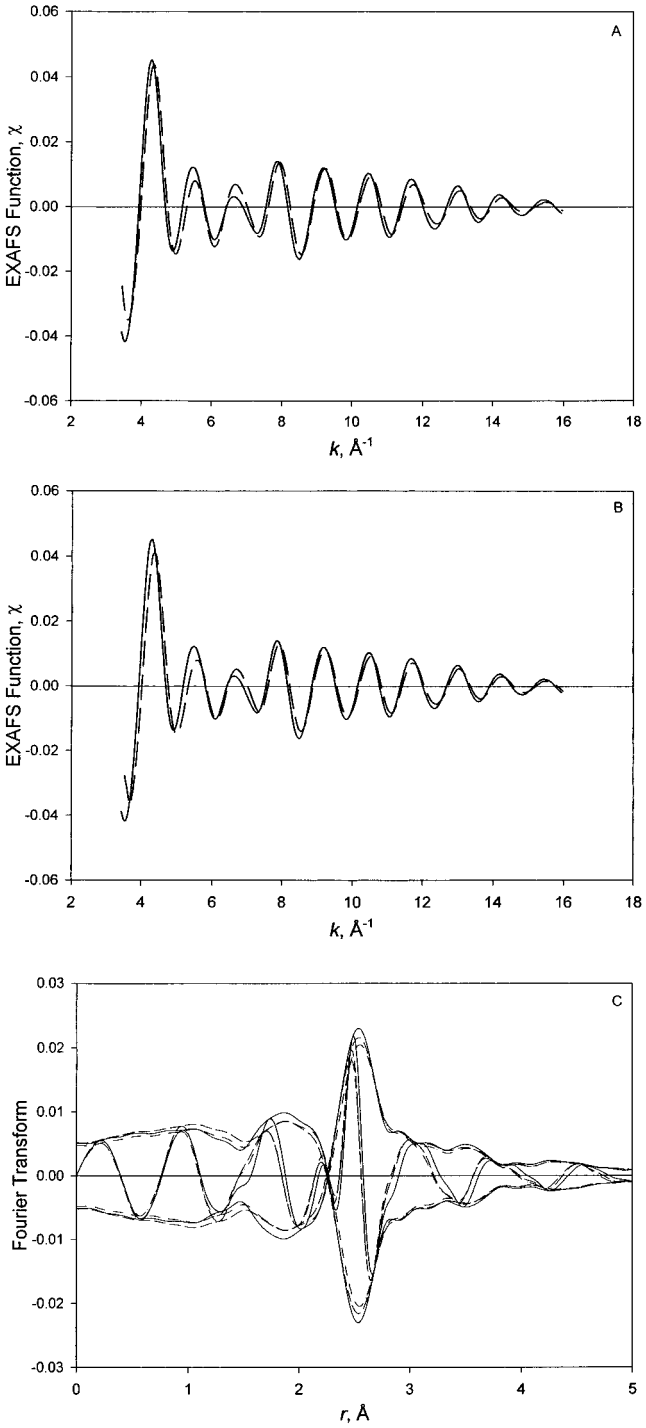

Figure 8. (A) Raw EXAFS data characterizing uncalcined NaY zeolite-supported rhodium carbonyl clusters formed from [$Rh(CO)_2$(acac)] in flowing CO at 125 °C and 2 atm for 12 h (dashed line) and crystalline [$Rh_6(CO)_{16}$] mixed with BN (solid line). (B) Raw EXAFS data characterizing NaY zeolite (calcined at 300 °C)-supported rhodium carbonyl clusters formed from [$Rh(CO)_2$(acac)] in flowing CO at 125 °C and 2 atm for 12 h (dashed line) and crystalline [$Rh_6(CO)_{16}$] mixed with BN (solid line). (C) Fourier transform of the raw EXAFS data characterizing uncalcined (dashed line) and calcined (dash−dotted line) NaY zeolite-supported rhodium carbonyl clusters formed from [$Rh(CO)_2$(acac)] in flowing CO at 125 °C and 2 atm for 12 h and crystalline [$Rh_6(CO)_{16}$] mixed with BN (solid line).

2020 m cm^{-1} and a face-bridging CO band at 1765 cm^{-1}; the latter spectrum is nearly the same as that of the original sample before decarbonylation, indicating that [$Rh_6(CO)_{16}$] was reformed and that the decarbonylation was reversible (Figure 7). The recarbonylated sample was grayish-pink in color.

TABLE 4: X-ray Data Characterizing Rhodium Clusters[a]

		XRD parameters[b]		EXAFS parameters[b]			
sample	backscatterer	N	R, Å	N	R, Å	$\Delta\sigma^2$, Å^2	ΔE_0, eV
$[Rh_6(CO)_{16}]$	Rh	4	2.776				
	C_t	2	1.864				
	C_{fb}	2	2.168				
	O^*_{avg}	4	3.061				
$[Rh_6(CO)_{16}]$ mixed with BN	Rh			4.1	2.77	−0.001 17	2.27
	C_t			2.4	1.87	0.002 02	9.35
	O^*_t			2.6	2.82	0.002 30	25.0
	C_{fb}			3.2	2.18	0.008 60	−9.73
	O^*_{fb}			3.5	2.96	0.007 71	−9.50
$[Rh_6(CO)_{16}]$ in uncalcined NaY zeolite[c]	Rh			3.8	2.76	−0.000 19	2.27
	C_t			2.5	1.86	0.004 15	9.35
	O^*_t			2.4	2.78	0.005 11	21.7
	C_{fb}			3.2	2.14	0.015 00	−9.76
	O^*_{fb}			3.3	2.91	−0.002 25	−1.95
$[Rh_6(CO)_{16}]$ NaY zeolite calcined at 200 °C	Rh			3.4	2.76	−0.000 82	4.43
	C_t			2.9	1.86	0.004 18	8.48
	O^*_t			1.7	2.85	0.003 97	15.64
	C_{fb}			3.3	2.18	0.008 77	−9.87
	O^*_{fb}			3.1	2.91	−0.003 57	−6.14
$[Rh_6(CO)_{16}]$ NaY zeolite calcined at 300 °C	Rh			3.2	2.76	−0.000 78	3.15
	C_t			1.9	1.85	0.002 41	8.62
	O^*_t			2.0	2.75	0.005 03	25.0
	C_{fb}			2.7	2.13	0.017 73	−9.84
	O^*_{fb}			3.1	2.91	−0.003 56	−6.14

[a] Notation: R, absorber(Rh)−backscatterer distance; $\Delta\sigma$,[2] Debye−Waller factor; ΔE_0, inner potential correction. Subscripts: t, terminal; fb, face-bridging; avg, average. Other terms defined in Table 1. [b] Reference 25. [c] See text for estimate of purity.

EXAFS Evidence of $[Rh_6(CO)_{16}]$ in NaY Zeolite. The raw EXAFS data characterizing the samples formed from the uncalcined and calcined zeolites, following treatment in CO, are compared in Figure 8 with the raw EXAFS data characterizing pure $[Rh_6(CO)_{16}]$ in BN. The data show oscillations up to values of k of about 16 Å^{-1}, consistent with the presence of Rh−Rh contributions. The number of scans done for each sample, along with the standard deviations in the EXAFS functions over the k range fitted, are summarized in Table 2. The Fourier transforms of the raw EXAFS data characterizing $[Rh_6(CO)_{16}]$ mixed with BN, in calcined zeolite, and in uncalcined zeolite are shown in Figure 8C.

The EXAFS data characterizing NaY zeolite samples, uncalcined and calcined, with infrared spectra indicative of $[Rh_6(CO)_{16}]$ were fitted according to each of the three models discussed in the section EXAFS Data Analysis. The structural parameters representing the third (and best) model are summarized in Table 4, and the comparisons of the data and the fits, in k space and in r space, are shown in Figure 9A,B (only for the uncalcined zeolite).

Characterization of Decarbonylated Rhodium Clusters by EXAFS Spectroscopy. The raw EXAFS data characterizing the decarbonylated rhodium clusters formed by the treatment for 2 h of the uncalcined zeolite-supported $[Rh_6(CO)_{16}]$ in He or in H_2 at 200, 250, or 300 °C show oscillations up to values of k equal to about 16 Å^{-1}, consistent with Rh−Rh contributions and the presence of rhodium clusters in the zeolite (Figures 10−13).

The EXAFS data characterizing the rhodium clusters formed by decarbonylation in He could be fitted satisfactorily only by inclusion of a contribution with a short Rh−O distance (2.1 Å) and a Rh−Rh contribution, at 2.69 Å (Table 5, Figures 10 and 11). A Rh−C contribution could be fitted as well (at about 1.95 Å) with a coordination number typically ≤0.5 (and this contribution was so small that it had little effect on the overall fit), indicating that decarbonylation was nearly complete. The analysis of the EXAFS data characterizing the sample treated in H_2 (Table 6, Figures 12 and 13) also indicates the presence of a Rh−Rh contribution (at 2.68 Å); in addition, the analysis indicates Rh−O and Rh−C contributions, with distances of 2.11 and 1.97 Å, respectively. The k range used in the fitting and the standard deviations in the EXAFS function for each decarbonylated sample are stated in Table 2.

Discussion

Analogy between Rhodium Carbonyl Chemistry in Zeolite Cages and in Solution. *Formation of Rhodium Carbonyls under Neutral Conditions.* The reactions of rhodium carbonyls in neutral solutions usually give neutral products. For example, $[Rh(CO)_2Cl]_2$ reacts with CO and H_2O in aqueous methanol to give the dark brown $[Rh_4(CO)_{12}]$ and the red $[Rh_6(CO)_{16}]$, represented by eqs 1 and 2, respectively:[33]

$$2Rh_2(CO)_4Cl_2 + 6CO + 2H_2O \rightarrow [Rh_4(CO)_{12}] + 2CO_2 + 4HCl \quad (1)$$

$$Rh_2(CO)_4Cl_2 + 7CO + 3H_2O \rightarrow [Rh_6(CO)_{16}] + 3CO_2 + 6HCl \quad (2)$$

Analogous chemistry is illustrated by the formation of $[Rh_4(CO)_{12}]$ and $[Rh_6(CO)_{16}]$ in the pores of NaY zeolite,[7−10] by the formation of $[Rh_6(CO)_{16}]$ on the surface of Al_2O_3,[34] and by the formation of $[Ir_4(CO)_{12}]$ on the surface of γ-Al_2O_3[35] and in the pores of NaY zeolite.[11] Several authors[7−10] investigated the synthesis of $[Rh_6(CO)_{16}]$ by the reductive carbonylation of rhodium cations in the pores of NaY zeolite. The synthesis conditions are summarized in Table 7; because typical precursors were rhodium chloride salts, chloride ions remained in the zeolites. All these syntheses involved the reduction of Rh(III) to Rh(I) and then to the Rh(0) of $[Rh_6(CO)_{16}]$. The final reaction in this reduction has been suggested to require the presence of water.[10,34] It is also known from the solution chemistry that chloride ions may lower the rate of reduction of rhodium cations and influence what rhodium carbonyl is ultimately formed.

The results presented here demonstrate the suitability of $[Rh(CO)_2(acac)]$ as a precursor for the synthesis of supported

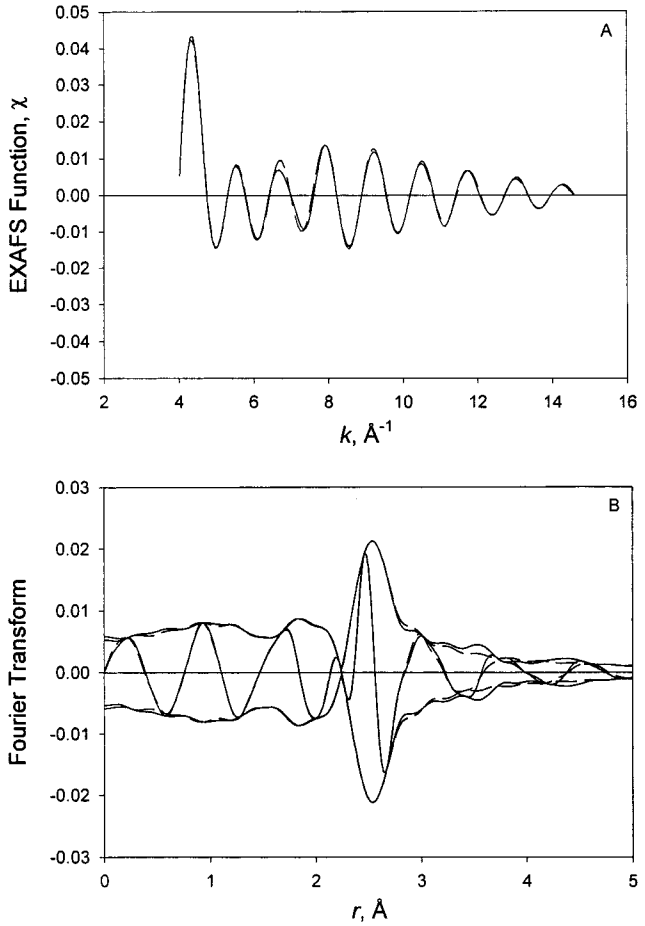

Figure 9. Results of EXAFS analysis characterizing sample initially containing $[Rh(CO)_2(acac)]$ in NaY zeolite after treatment in CO at 125 °C and 2 atm for 12 h: (A) raw EXAFS function (solid line) and sum of the calculated Rh−Rh + Rh−C_t + Rh−C_{fb} + Rh−O* contributions (dashed line); (B) imaginary part and magnitude of Fourier transform (unweighted; $\Delta k = 4-14.7$ Å) of raw EXAFS function (solid line) and sum of the calculated Rh−Rh + Rh−C_t + Rh−C_{fb} + Rh−O* contributions (dashed line) (terms defined in Table 4).

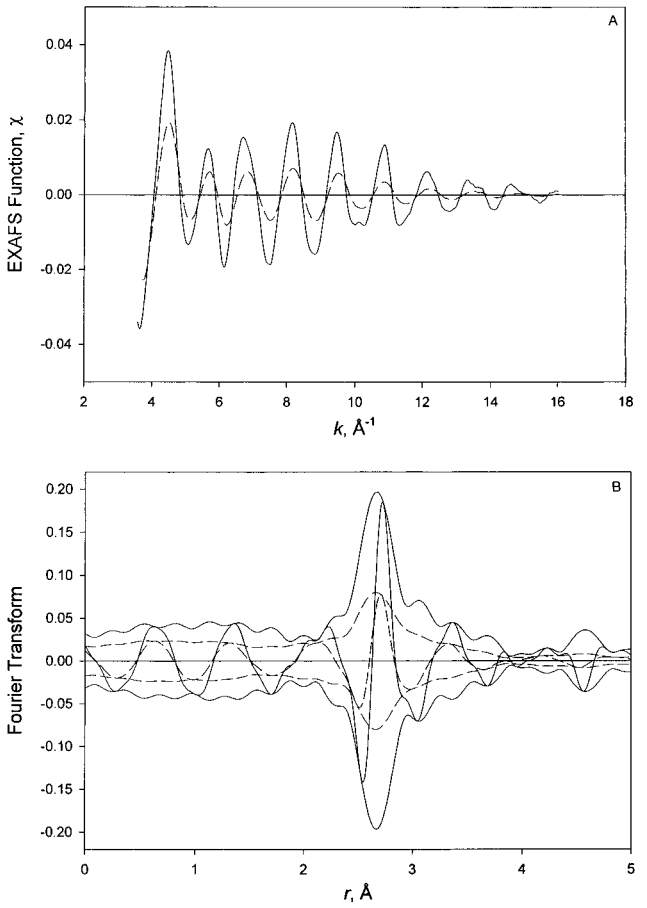

Figure 10. (A) Raw EXAFS data characterizing uncalcined NaY zeolite-supported (solid line) and NaY zeolite (calcined at 300 °C)-supported (dashed line) rhodium clusters formed by the decarbonylation of $[Rh_6(CO)_{16}]$ at 200 °C in the presence of He. (B) Fourier transforms, phase and amplitude corrected with data characterizing Rh foil, of raw EXAFS data characterizing uncalcined NaY zeolite-supported (solid line) and NaY zeolite (calcined at 300 °C)-supported (dashed line) rhodium clusters formed by the decarbonylation of $[Rh_6(CO)_{16}]$ at 200 °C in the presence of He.

$[Rh_6(CO)_{16}]$; the principal advantage of this precursor is that it avoids chloride or other anions that would remain on the support after the synthesis.

$[Rh_6(CO)_{16}]$ in NaY Zeolite. The infrared evidence of $[Rh_6(CO)_{16}]$ in uncalcined NaY zeolite is consistent with infrared evidence reported by several authors[7−10] indicating this cluster in the zeolite (Table 3). The shifts of the terminal and bridging carbonyl bands observed for $[Rh_6(CO)_{16}]$ in NaY zeolite relative to those of $[Rh_6(CO)_{16}]$ in chloroform solution match the qualitative pattern illustrated by the shifts of the comparable bands in the spectra of $[Ir_6(CO)_{16}]$ and of $[Ir_4(CO)_{12}]$ in NaY zeolite relative to those of the compounds in solution.[11,12] Similar shifts have been observed for metal carbonyls in solutions containing Lewis acids such as $Al(C_2H_5)_3$.[36,37] The shifts are explained by interactions of the face-bridging CO ligands with Lewis acid sites of the zeolite. Interaction of a metal carbonyl with a Lewis acid through the oxygen atom of a carbonyl group typically results in a substantial decrease of the CO stretching frequency, with the frequencies of the noninteracting carbonyl ligands all shifting to slightly higher values.

The structure parameters determined from the EXAFS data characterizing the sample inferred to consist of $[Rh_6(CO)_{16}]$ in NaY zeolite (Table 4, Figure 8) agree well with the structural data determined for crystalline $[Rh_6(CO)_{16}]$ by X-ray diffraction[25] and EXAFS spectroscopy (Table 4), confirming the conclusion that this cluster formed in the zeolite. A comparison of the EXAFS data for various samples containing $[Rh_6(CO)_{16}]$ (Table 4, Figure 8C) shows that the Rh−Rh coordination number was greatest for the crystalline $[Rh_6(CO)_{16}]$, less for the clusters in the uncalcined zeolite, and least for the clusters in the calcined zeolite. The qualitative shapes of the Fourier transforms of the raw EXAFS data characterizing $[Rh_6(CO)_{16}]$ in calcined and uncalcined NaY zeolites are virtually the same as that of $[Rh_6(CO)_{16}]$ in BN. Furthermore, the phases of the imaginary parts of the EXAFS functions characterizing supported $[Rh_6(CO)_{16}]$ and $[Rh_6(CO)_{16}]$ are nearly identical.

As both the infrared and EXAFS data are consistent with the presence of $[Rh_6(CO)_{16}]$ in the samples, we interpret the results as evidence of the yields of $[Rh_6(CO)_{16}]$. The percentage yields of $[Rh_6(CO)_{16}]$ were estimated by dividing the Rh−Rh coordination number determined for the sample containing the supported clusters by 4 (which is the Rh−Rh coordination number of $[Rh_6(CO)_{16}]$) and multiplying by 100. These estimates are based on the assumption that all rhodium not in the form of $[Rh_6(CO)_{16}]$ is characterized by a Rh−Rh coordination number of 0, corresponding to mononuclear rhodium complexes. Because there is no evidence of edge-bridging carbonyl ligands in the rhodium carbonyls in the calcined sample, it seems appropriate to assume that the rhodium not present in $[Rh_6(CO)_{16}]$ was present in species of low nuclearity, such as mononuclear species.

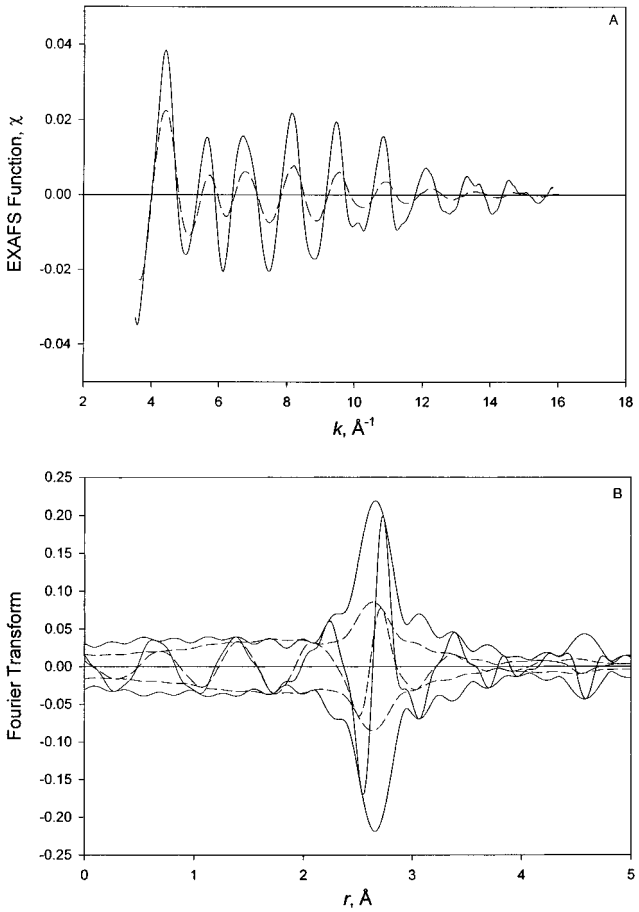

Figure 11. (A) Raw EXAFS data characterizing uncalcined NaY zeolite-supported (solid line) and NaY zeolite (calcined at 300 °C)-supported (dashed line) rhodium clusters formed by the decarbonylation of $[Rh_6(CO)_{16}]$ at 300 °C in the presence of He. (B) Fourier transforms, phase and amplitude corrected with data characterizing Rh foil, of raw EXAFS data characterizing uncalcined NaY zeolite-supported (solid line) and NaY zeolite (calcined at 300 °C)-supported (dashed line) rhodium clusters formed by the decarbonylation of $[Rh_6(CO)_{16}]$ at 300 °C in the presence of He.

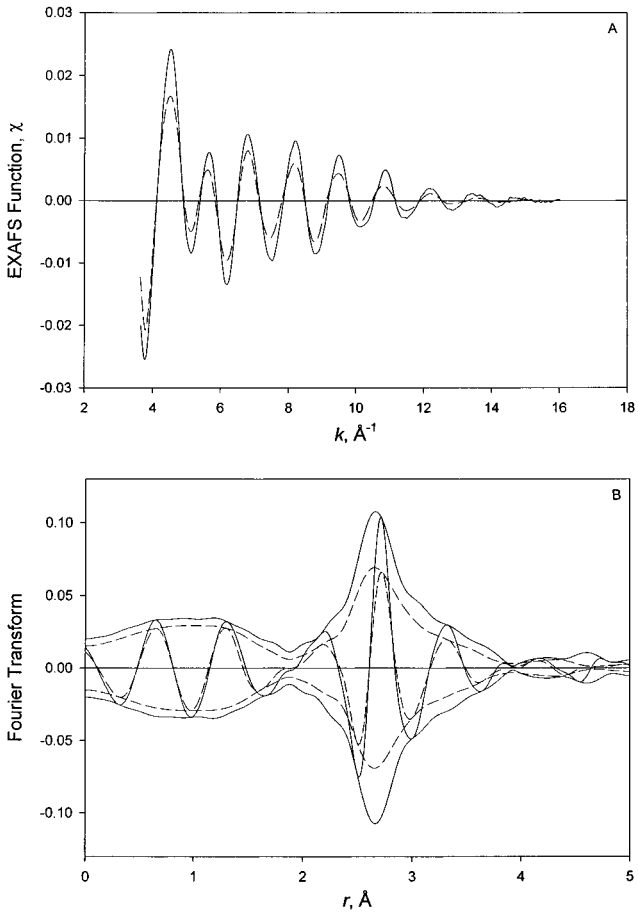

Figure 12. (A) Raw EXAFS data characterizing uncalcined NaY zeolite-supported (solid line) and NaY zeolite (calcined at 300 °C)-supported (dashed line) rhodium clusters formed by the decarbonylation of $[Rh_6(CO)_{16}]$ at 200 °C in the presence of H_2. (B) Fourier transforms, phase and amplitude corrected with data characterizing Rh foil, of raw EXAFS data characterizing uncalcined NaY zeolite-supported (solid line) and NaY zeolite (calcined at 300 °C)-supported (dashed line) rhodium clusters formed by the decarbonylation of $[Rh_6(CO)_{16}]$ at 200 °C in the presence of H_2.

The EXAFS data lead to the following estimates: the yield of $[Rh_6(CO)_{16}]$ in the uncalcined zeolite was greater than 90%, and the yield of $[Rh_6(CO)_{16}]$ in the calcined zeolite was about 80% (Table 8). The yields inferred from the EXAFS data are supported qualitatively by the infrared spectra (Figure 3) showing relatively high intensities of υ_{CO} bands associated with rhodium subcarbonyls in the calcined samples, consistent with the inference that the calcined samples were characterized by relatively low conversions of supported $Rh(I)(CO)_2$ species into $[Rh_6(CO)_{16}]$.

Quasimolecular Rhodium Clusters Formed by Decarbonylation of NaY Zeolite-Supported $[Rh_6(CO)_{16}]$. The infrared spectra show that decarbonylation of $[Rh_6(CO)_{16}]$ in the zeolite calcined at 300 °C was nearly complete after 2 h in flowing He at 200 °C and complete at 250 °C. The EXAFS data provide structural information about the decarbonylated clusters. The Rh−Rh coordination number characterizing the decarbonylated clusters (Table 9) is nearly 4, the value characteristic of the precursor identified as predominantly $[Rh_6(CO)_{16}]$ (Table 4). Because the coordination numbers of the supported rhodium carbonyls and the clusters formed by their decarbonylation are nearly the same, we infer that the cluster nuclearity of the rhodium carbonyls was preserved during decarbonylation. Thus we conclude that clusters approximated as hexarhodium formed in the zeolite cages. Furthermore, the EXAFS data characterizing the partially decarbonylated clusters in NaY zeolite (which formed as a result of treatment in H_2 of $[Rh_6(CO)_{16}]$ in the zeolite that had been calcined at 200 or 300 °C) retained or nearly retained the Rh−Rh coordination number of about 4; again, we infer that the nuclearity of the clusters was nearly 6 (Table 9). On the basis of these results, we infer that the family of supported metal clusters with relatively well-defined and almost molecular structures has been extended to include rhodium.

The decarbonylation of $[Rh_6(CO)_{16}]$ supported in the NaY zeolite sample that had been calcined at 200 °C, with the decarbonylation occurring in the presence of He at 200, 250, 300, or 400 °C, resulted in clusters having metal−metal coordination numbers between 4.3 and 4.9. These clusters are thus larger than Rh_6, having nuclearities in the range of about 6−20 atoms and no doubt being structurally nonuniform (Table 9). It follows that aggregation of the rhodium accompanied decarbonylation in these samples. Clusters of similar size were also formed in uncalcined NaY zeolite when the supported $[Rh_6(CO)_{16}]$ was partially decarbonylated in H_2 at 200 °C, resulting in a Rh−Rh coordination of about 4.5. These results suggest that migration of rhodium carbonyls through the zeolite pores took place after a fraction of the CO ligands had been removed, making the effective cluster diameter less than the diameter of the windows connecting the supercages of the zeolite. Evidence of migration of metal carbonyls on hydroxylated metal oxide surfaces has been reported before.[39]

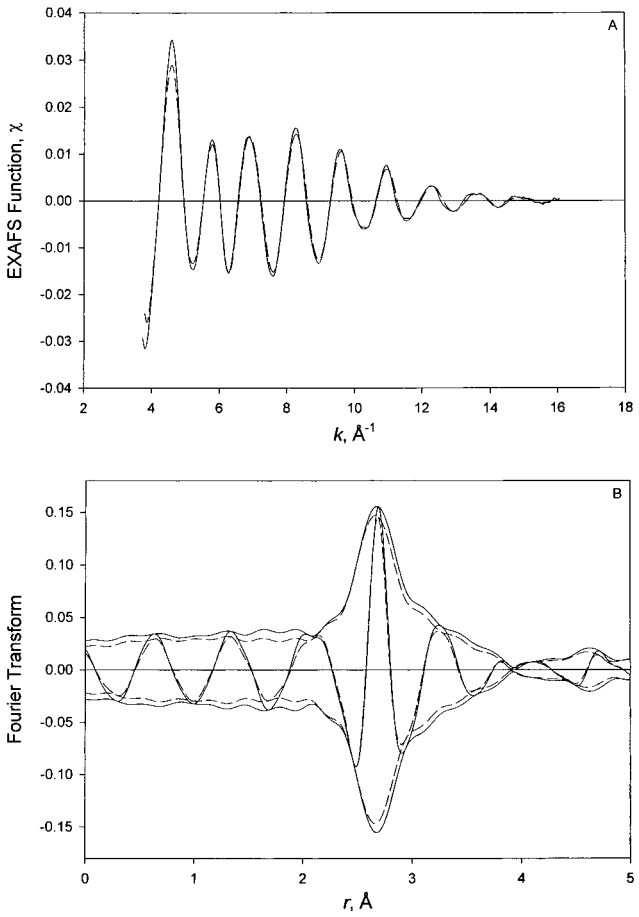

Figure 13. (A) Raw EXAFS data characterizing uncalcined NaY zeolite-supported (solid line) and NaY zeolite (calcined at 300 °C)-supported (dashed line) rhodium clusters formed by the decarbonylation of $[Rh_6(CO)_{16}]$ at 300 °C in the presence of H_2. (B) Fourier transforms, phase and amplitude corrected with data characterizing Rh foil, of raw EXAFS data characterizing uncalcined NaY zeolite-supported (solid line) and NaY zeolite (calcined at 300 °C)-supported (dashed line) rhodium clusters formed by the decarbonylation of $[Rh_6(CO)_{16}]$ at 300 °C in the presence of H_2.

The Rh−Rh bonding distances determined for the clusters formed as stated above ranged from 2.67 to 2.69 Å. One would expect the Rh−Rh bonding distance in small rhodium clusters to be slightly less than the bulk rhodium bonding distance (2.69 Å), provided that the clusters did not interact with adsorbates such as CO or hydrogen. However, the experimental error in the distances (± approximately 1%) is larger than this difference; thus, we cannot distinguish between the observed Rh−Rh bonding distances in the clusters and that in bulk rhodium. The above bonding distances are consistent with the findings of other groups for quasimolecular clusters of Rh in NaY zeolite and on SiO_2.[7,40]

The EXAFS data fits characterizing the supported clusters show evidence of a Rh−O contribution at about 2.1 Å and a Rh−C contribution at about 1.95 Å. The data characterizing each of the samples that had been partially decarbonylated in H_2 showed a significant Rh−C contribution ($N > 1$), whereas those clusters formed by decarbonylation showed only a very small Rh−C contribution ($N > 0.5$). The signals indicative of these contributions are rather weak in comparison with that indicative of the Rh−Rh contribution; furthermore, the reference files used to analyze each of these contributions may not as accurately describe the Rh−O and Rh−C interactions as the data characterizing rhodium foil represent the Rh−Rh contribution. Therefore, significant errors are expected in both the Rh−O and Rh−C coordination numbers (we estimate as much as roughly ± 50%) and distances (we estimate as much as about ± 10%). Because Rh−Na, Rh−Al, and Rh−Si contributions likely affect the EXAFS spectra for values of $k < 10$ Å and are not accounted for in the fit, these add to the uncertainty in the values of R and N characterizing the Rh−C and Rh−O contributions.

Formation of Aggregated Rh Particles Supported on NaY Zeolite. Decarbonylation of $[Rh_6(CO)_{16}]$ in uncalcined NaY zeolite in the presence of He at 200, 250, or 300 °C resulted in samples characterized by Rh−Rh coordination numbers of 6 or greater, indicative of rhodium clusters or particles having nuclearities larger than about 30 atoms, on average. Similarly, rhodium clusters or particles were formed in uncalcined NaY zeolite when decarbonylation occurred in H_2 at 250 or 300 °C. At least some of the rhodium clusters or particles in these samples are inferred to have been too large to fit in the zeolite supercages; they must have existed outside the intracrystalline zeolite pores (Table 9).

Besides fitting the first-shell Rh−Rh contribution, we were able to fit the remainder of the EXAFS data with a Rh−O contribution. However, because the magnitude of the Rh−O contribution was of the order of the noise in the data, it was not possible to determine the Rh−O coordination number accurately. Therefore, all that can be stated is that a Rh−O contribution likely exists at about 2.1 Å with a coordination number less than that observed for the quasimolecular clusters referred to above.

Recarbonylation of Rhodium Clusters in NaY Zeolite. When CO was dosed into the zeolite sample containing rhodium clusters that had been formed by partial decarbonylation in H_2 at 200 °C, $[Rh_6(CO)_{16}]$ formed again, as shown by the relative intensities and position of the υ_{CO} bands in the infrared spectrum and by the color, which nearly match those of the original rhodium carbonyl clusters (Figure 7). The reversibility of the partial decarbonylation of $[Rh_6(CO)_{16}]$ suggests that the partially decarbonylated clusters were still hexanuclear. The EXAFS data (Table 6) agree with the inference that hexanuclear clusters were present, possibly mixed with larger rhodium clusters as well as mononuclear rhodium species.

The mechanism of reconstruction of $[Rh_6(CO)_{16}]$ from the decarbonylated sample is not known. The literature of rhodium carbonyls on Al_2O_3[34] and that of iridium carbonyls in NaY zeolite[11] indicate that rhodium clusters in the presence of water or surface OH groups are oxidatively fragmented by CO to give mononuclear rhodium subcarbonyls, $Rh^+(CO)_2$, which, upon further treatment in CO, give $[Rh_6(CO)_{16}]$. When the samples containing the larger clusters and particles were treated in CO in the infrared cell at 125 °C, bands were observed at 2068 cm^{-1}, indicative of linearly bonded CO on rhodium, and at 2110, 2090, 2048, and 2020 cm^{-1}, indicative of $Rh^+(CO)_2$ species formed by oxidative fragmentation.[41,42] It has been shown that when zeolite-supported rhodium clusters or particles consisting of more than six atoms each are exposed to CO, the rhodium atoms are oxidized to $Rh^+(CO)_2$ and Rh^{3+} ions.[41−43] Because this fast oxidative fragmentation requires the presence of surface OH groups or water, the rate becomes negligible when these groups are exhausted.[44] At this point the pathway to reformation of $[Rh_6(CO)_{16}]$ becomes blocked.

In contrast, $[Rh_6(CO)_{16}]$ did not reform when CO was dosed into the zeolite sample containing rhodium clusters that had been formed by decarbonylation in He at 200 °C, as shown by the relative intensities and positions of the υ_{CO} bands in the infrared spectrum and by the color, which was gray and not pink like that of the original rhodium carbonyl clusters (Figure 7). The resultant spectrum is similar to a spectrum reported by Rao et

TABLE 5: EXAFS Results Characterizing Rhodium Clusters Supported on NaY Zeolite[a] Formed by Decarbonylation of $[Rh_6(CO)_{16}]$ in He

support preparation conditions[b]			conditions of treatment of sample containing $[Rh_6(CO)_{16}]$				EXAFS Parameters			
treatment gas	temp, °C	time, h	treatment gas	temp, °C	time, h	backscatterer	*N*	*R*, Å	$\Delta\sigma^2$, Å^2	ΔE_0, eV
	25		He	200	2	Rh	7.4	2.69	0.001 83	4.81
						O		2.08		
	25		He	250	2	Rh	7.5	2.69	0.001 05	4.52
						O		2.10		
	25		He	300	2	Rh	8.0	2.69	0.001 71	5.80
						O		2.20		
O_2	200	4	He	200	2	Rh	4.6	2.68	0.003 64	4.27
						O	0.9	2.12	0.012 00	−12.53
O_2	200	4	He	250	2	Rh	4.3	2.68	0.003 82	6.25
						O	1.5	2.12	0.013 00	−13.69
O_2	200	4	He	300	2	Rh	4.4	2.67	0.002 96	3.78
						O	1.6	2.12	0.015 00	−16.98
O_2	200	4	He	400	2	Rh	4.9	2.67	0.002 60	0.58
						O	1.3	2.09	0.010 36	−5.18
O_2	300	4	He	200	2	Rh	3.8	2.68	0.003 76	2.89
						O	1.2	2.12	0.015 00	−12.24
O_2	300	4	He	250	2	Rh	3.5	2.69	0.003 99	4.09
						O	1.3	2.10	0.013 38	−3.25
O_2	300	4	He	300	2	Rh	3.9	2.68	0.003 91	4.37
						O	1.1	2.17	0.007 26	−10.01
O_2	300	4	He	400	2	Rh	4.5	2.67	0.002 84	1.20
						O	0.9	2.12	0.005 29	−7.80

[a] Notation: *R*, absorber(Rh)−backscatterer distance; $\Delta\sigma^2$, Debye−Waller factor; ΔE_0, inner potential correction. Other terms defined in Table 1. [b] All samples were evacuated at treatment temperature for 12 h (following gas treatment for samples treated in O_2).

TABLE 6: EXAFS Results Characterizing Rhodium Clusters Supported on NaY Zeolite[a] Formed by Decarbonylation of $[Rh_6(CO)_{16}]$ in H_2

support preparation conditions[b]			conditions of treatment of sample containing $[Rh_6(CO)_{16}]$				EXAFS Parameters			
treatment gas	temp, °C	time, h	treatment gas	temp, °C	time, h	backscatterer	*N*	*R*, Å	$\Delta\sigma^2$, Å^2	ΔE_0, eV
	25		H_2	200	2	Rh	4.5	2.68	0.003 50	3.94
						O	1.0	2.12	0.008 25	−14.58
						C	1.1	1.91	0.005 35	−1.79
	25		H_2	250	2	Rh	6.0	2.68	0.004 05	5.70
						O	1.4	2.05	0.011 46	−7.81
						C	0.7	1.82	0.004 57	−9.70
	25		H_2	300	2	Rh	7.5	2.68	0.003 92	5.30
						O	0.8	2.15	0.006 14	−17.15
						C				
O_2	200	4	H_2	200	2	Rh	3.3	2.69	0.004 77	6.06
						O	1.0	2.13	0.005 90	−14.49
						C	1.2	1.91	0.003 82	−1.77
O_2	200	4	H_2	250	2	Rh	3.6	2.69	0.005 16	4.42
						O	1.5	2.09	0.012 37	−7.98
						C	0.9	1.92	0.001 33	−6.39
O_2	200	4	H_2	300	2	Rh	6.8	2.68	0.003 65	2.23
						O	1.3	2.09	0.010 00	−15.14
						C				
O_2	300	4	H_2	200	2	Rh	3.5	2.68	0.004 45	5.94
						O	0.7	2.12	0.004 76	−14.56
						C	1.1	1.91	0.003 45	−1.77
O_2	300	4	H_2	250	2	Rh	3.8	2.68	0.004 41	2.61
						O	1.0	2.10	0.008 02	−12.04
						C	0.7	1.91	0.002 83	−9.18
O_2	300	4	H_2	300	2	Rh	6.7	2.68	0.003 48	1.92
						O	1.0	2.06	0.010 00	−11.24

[a] Notation: *R*, absorber(Rh)−backscatterer distance; $\Delta\sigma^2$, Debye−Waller factor; ΔE_0, inner potential correction. Other terms defined in Table 1. [b] All samples were evacuated at treatment temperature for 12 h (following gas treatment for samples treated in O_2).

al.[45] (obtained after a different set of treatments), which they identified with $Rh_6(CO)_{12}(\mu_2\text{-}CO)_4$ (where μ_2 denotes edge-bridging CO ligands). However, in light of the large Rh−Rh coordination number characterizing the clusters formed by decarbonylation in He, it is unlikely that rhodium clusters with a nuclearity of 6 formed, in contrast to the suggestion of Rao et al.[45]

Conclusions

NaY zeolite-supported rhodium carbonyls, with the predominant species being $[Rh_6(CO)_{16}]$, were prepared by carbonylation of $[Rh(CO)_2(acac)]$ in the zeolite supercages. Uncalcined NaY zeolite containing $[Rh(CO)_2(acac)]$ gave a higher yield of $[Rh_6(CO)_{16}]$ than the calcined zeolite, consistent with the role of water in the cluster synthesis. Decarbonylation of $[Rh_6$-

TABLE 7: Summary of Conditions of Synthesis of $[Rh_6(CO)_{16}]$ in NaY Zeolite

precursor	treatment gas	temp, °C	pressure, atm	ref
$[Rh_6(CO)_{16}]$	CO	125	1	6
$RhCl_3 \cdot 3H_2O$	$CO:H_2O$ (120:1)[a]	120	1	7
$[Rh(NH_3)_6]Cl_3$	$CO:H_2$ (1:1)[a]	130	80	8
$RhCl_3 \cdot 3H_2O$	CO	125	3	9, 10
$[Rh(CO)_2(acac)]$	CO	125	1−2	this work

[a] Molar ratio.

TABLE 8: Yields of $[Rh_6(CO)_{16}]$ in NaY Zeolite Calculated from Rh−Rh Coordination Number Determined from EXAFS Spectroscopy

support	N_{Rh-Rh}[a]	yield, %[b]
NaY zeolite (uncalcined)	3.8	95
NaY zeolite calcined at 200 °C	3.4	85
NaY zeolite calcined at 300 °C	3.2	80

[a] Rh−Rh coordination number determined by EXAFS spectroscopy (Table 4). [b] Yield $= (N_{Rh-Rh}/4) \times 100$.

TABLE 9: Rhodium Clusters Formed by Decarbonylation of $[Rh_6(CO)_{16}]$ Supported in NaY Zeolite[a]

support preparation conditions[b]			conditions of treatment of sample containing $[Rh_6(CO)_{16}]$				
treatment gas	temp, °C	time, h	treatment gas	temp, °C	time, h	N_{Rh-Rh}	approx cluster nuclearity[c]
O_2	200	4	H_2	200	2	3.3	6
O_2	200	4	H_2	250	2	3.6	6
O_2	300	4	H_2	200	2	3.5	6
O_2	300	4	H_2	250	2	3.8	6
O_2	300	4	He	200	2	3.8	6
O_2	300	4	He	250	2	3.5	6
O_2	300	4	He	300	2	3.9	6
none	25	0	H_2	200	2	4.5	6−10
O_2	200	4	He	200	2	4.6	6−10
O_2	200	4	He	250	2	4.3	6−10
O_2	200	4	He	300	2	4.4	6−10
O_2	200	4	He	400	2	4.9	6−10
O_2	300	4	He	400	2	4.5	6−10
none	25	0	H_2	250	2	6.0	20
O_2	200	4	H_2	300	2	6.8	30
O_2	300	4	H_2	300	2	6.7	30
none	25	0	H_2	300	2	7.5	50
none	25	0	He	200	2	7.4	50
none	25	0	He	250	2	7.5	50
none	25	0	He	300	2	8.0	70

[a] Notation as in Table 1. [b] All samples were evacuated at treatment temperature for 12 h (following gas treatment for samples treated in O_2). [c] Reference 38.

$(CO)_{16}]$ in the zeolite calcined at 300 °C gave a sample shown by EXAFS spectroscopy to have a Rh−Rh coordination number of nearly 4; thus, the clusters in this sample are represented as Rh_6. Because the EXAFS data characterizing these samples showed no significant difference between the Rh−Rh coordination number of the metal carbonyl precursor, $[Rh_6(CO)_{16}]$, and the Rh−Rh coordination number of the clusters formed by decarbonylation, it is inferred that rhodium was present predominantly as Rh_6 clusters (with some mononuclear species). The EXAFS data also indicate hexarhodium clusters among the partially decarbonylated clusters in NaY zeolite formed by treatment of $[Rh_6(CO)_{16}]$ in H_2. These samples could be recarbonylated to give back $[Rh_6(CO)_{16}]$. In contrast, other samples of $[Rh_6(CO)_{16}]$ in NaY zeolite gave larger clusters and particles of rhodium upon decarbonylation, and the aggregates of rhodium did not give back $[Rh_6(CO)_{16}]$ upon recarbonylation.

Acknowledgment. The research was supported by the U.S. Department of Energy, Office of Energy Research, Office of Basic Energy Sciences, Division of Chemical Sciences, Contract No. FG02-87ER13790. We acknowledge the support of the U.S. Department of Energy, Division of Materials Sciences, under contract number DE-FG05-89ER45384, for its role in the operation and development of beam line X-11A at the National Synchrotron Light Source (NSLS). The NSLS is supported by the Department of Energy, Division of Materials Sciences and Division of Chemical Sciences, under Contract No. DE-AC02-76CH00016. We thank the staff of beam line X-11A for their assistance. The X-ray absorption data were analyzed with the XDAP software.[46]

References and Notes

(1) Psaro, R.; Ugo, R. In *Metal Clusters in Catalysis*; Gates, B. C., Guczi, L., Knözinger, H., Eds.; Elsevier: Amsterdam, 1986.
(2) Vaarkamp, M.; Mojet, B. L.; Kappers, M. J.; Miller, J. T.; Koningsberger, D. C. *J. Phys. Chem.* **1995**, *99*, 16067.
(3) *Oil Gas J.* **1992**, *190*, 29.
(4) Gates, B. C. *Chem. Rev. (Washington, D.C.)* **1995**, *95*, 511.
(5) Moller, K.; Koningsberger, D. C.; Bein, T. *J. Phys. Chem.* **1989**, *93*, 6116.
(6) Gelin, P.; Ben Taarit, Y.; Naccache, C. *J. Catal.* **1979**, *59*, 357.
(7) Rao, L.-F.; Fukuoka, A.; Kosugi, N.; Kuroda, H.; Ichikawa, M. *J. Phys. Chem.* **1990**, *94*, 5317.
(8) Mantovani, E.; Palladino, N.; Zanobi, A. *J. Mol. Catal.* **1977**/**8**, *3*, 285.
(9) Davis, M. E.; Rode, E. J.; Taylor, D.; Hanson, B. E. *J. Catal.* **1984**, *86*, 67.
(10) Rode, E. J.; Davis, M. E.; Hanson, B. E. *J. Catal.* **1985**, *96*, 574.
(11) Beutel, T.; Kawi, S.; Purnell, S. K.; Knözinger, H.; Gates, B. C. *J. Phys. Chem.* **1993**, *97*, 7284.
(12) Kawi, S.; Chang, J.-R.; Gates, B. C. *J. Am. Chem. Soc.* **1993**, *115*, 4830.
(13) Jentoft, R. E.; Deutsch, S. E.; Gates, B. C. *Rev. Sci. Instrum.* **1996**, *67*, 2111.
(14) Zhao, A.; Gates, B. C. *J. Am. Chem. Soc.* **1996**, *118*, 2458.
(15) Duivenvoorden, F. B. M.; Koningsberger, D. C.; Uh, Y. S.; Gates, B. C. *J. Am. Chem. Soc.* **1986**, *108*, 6254.
(16) Teo, B.-K. *J. Am. Chem. Soc.* **1981**, *103*, 3990.
(17) Wyckoff, R. W. G., Ed. *Crystal Structures*, 2nd ed.; Wiley: New York, 1963; Vol. 1, p 10.
(18) Coey, J. M. D. *Acta Crystallogr.* **1970**, *B26*, 1876.
(19) Mason, R.; Rae, A. I. M. *J. Chem. Soc. A* **1968**, 778.
(20) van Zon, F. B. M.; Maloney, S. D.; Gates, B. C.; Koningsberger, D. C. *J. Am. Chem. Soc.* **1993**, *115*, 10317.
(21) van Zon, J. B. A. D. Ph.D. Dissertation, Eindhoven University of Technology, The Netherlands, 1988.
(22) van Zon, J. B. A. D.; Koningsberger, D. C.; van't Blik, H. F. J.; Sayers, D. E. *J. Chem. Phys.* **1985**, *82*, 5742.
(23) Kirlin, P. S.; van Zon, F. B. M.; Koningsberger, D. C.; Gates, B. C. *J. Phys. Chem.* **1990**, *94*, 8439.
(24) Koningsberger, D. C., Prins, R., Eds. *X-ray Absorption: Principles, Applications, Techniques of EXAFS, SEXAFS, and XANES;* Wiley: New York, 1988; p 395.
(25) Corey, E. R.; Dahl, L. F.; Beck, W. *J. Chem. Soc., Chem. Commun.* **1963**, *85*, 1202.
(26) van Zon, F. B. M.; Kirlin, P. S.; Gates, B. C.; Koningsberger, D. C. *J. Phys. Chem.* **1989**, *93*, 2218.
(27) Weber, W. A. Ph.D. Dissertation, University of California, Davis, in preparation.
(28) Shannon, R. D.; Vedrine, J. C.; Naccache, C.; Lefebvre, F. *J. Catal.* **1984**, *88*, 431.
(29) Hanson, B. E.; Davis, M. E.; Taylor, D.; Rode, E. *Inorg. Chem.* **1984**, *23*, 52.
(30) Lefebvre, F.; Ben Taarit, Y. *Nouv. J. Chim.* **1984**, *8*, 387.
(31) Wong, T. T.; Zhang, Z.; Sachtler, W. M. H. *Catal. Lett.* **1990**, *4*, 365.
(32) *Merck FT-IR Atlas*; Pachler, K. G. R., Matlok, F., Grendich, H.-U., Eds.; Merck: Darmstadt, VCH: Weinheim, 1988.
(33) Chini, P.; Martinengo, S. *Inorg. Chim. Acta* **1969**, *3*, 315.
(34) Smith, A. K.; Hugues, F.; Theolier, A.; Basset, J. M.; Ugo, R.; Zanderighi, G. M.; Bilhou, J. L.; Bilhou-Bougnol, V.; Graydon, W. F. *Inorg. Chem.* **1979**, *18*, 3104.
(35) Kawi, S.; Chang, J. R.; Gates, B. C. *J. Phys. Chem.* **1993**, *97*, 5375.
(36) Shriver, D. F. *J. Organomet. Chem.* **1975**, *94*, 259.

(37) Horwitz, C. P.; Shriver, D. F. *Adv. Organomet. Chem.* **1984**, *23*, 219.
(38) Kip, B. J.; Duivenvoorden, F. B. M.; Koningsberger, D. C.; Prins, R. *J. Catal*. **1987**, *105*, 26.
(39) Psaro, R.; Dossi, C.; Fusi, A.; Pergola, R.; Garlaschelli, L.; Roberto, D.; Sordelli, L.; Ugo, R.; Zanoni, R. *J. Chem. Soc., Faraday Trans.* **1992**, *88*, 369.
(40) Gloor, A. P.; Prins, R. *J. Phys. Chem.* **1994**, *98*, 9865.
(41) Bergeret, G.; Gallezot, P.; Gelin, P.; Ben Taarit, Y.; Lefebvre, F.; Naccache, C.; Shannon, R. D. *J. Catal.* **1987**, *104*, 279.
(42) Wong, T. T.; Stakheev, A. Y.; Sachtler, W. M. H. *J. Phys. Chem.* **1992**, *96*, 7733.
(43) van't Blik, H. F. J.; van Zon, J. B. A. D.; Huizinga, T.; Vis, J. C.; Koningsberger, D. C.; Prins, R. *J. Am. Chem. Soc.* **1985**, *107*, 3139.
(44) Wong, T. T.; Stakheev, A. Y.; Sachtler, W. M. H. *J. Phys. Chem.* **1992**, *96*, 7733.
(45) Rao, L.-F.; Pruski, M.; King, T. S. *J. Phys. Chem. B* **1997**, *101*, 5717.
(46) Vaarkamp, M.; Linders, J. C.; Koningsberger, D. C. *Physica B* **1995**, *209*, 159.